PERGAMON

Journal of Atmospheric and Solar-Terrestrial Physics 64 (2002) 291–305

Journal of ATMOSPHERIC AND SOLAR-TERRESTRIAL PHYSICS

www.elsevier.com/locate/jastp

Air–sea interface fluxes over the Indian Ocean during INDOEX, IFP-99

D. Bala Subrahamanyam, Radhika Ramachandran *

Space Physics Laboratory, Vikram Sarabhai Space Centre, Thiruvananthapuram, Kerala 695 022, India

Received 17 November 2000; received in revised form 22 June 2001; accepted 24 September 2001

Abstract

The Intensive Field Phase of Indian Ocean Experiment (INDOEX, IFP-99) was carried onboard Oceanic Research Vessel Sagar Kanya during January 20–March 12, 1999 over the latitudinal range 15°N–20°S and the longitudinal range 63°E–77°E. The present study deals with the spatial variation of air–sea fluxes over the Indian Ocean during the INDOEX, IFP-99 campaign. Drag coefficient (C_D), and sensible heat (C_H) and water vapor (C_E) exchange coefficients are determined using an iterative scheme. The estimated values of these coefficients are utilized for the computation of air–sea fluxes using the bulk aerodynamic method. The variations of air–sea flux estimates are studied with respect to the variation of wind speed.

Keywords: Air–sea fluxes; Bulk aerodynamic method; Indian Ocean experiment (INDOEX); Inter-tropical convergence zone (ITCZ); Marine atmospheric boundary layer (MABL); Marine meteorology

1. Introduction

More than 70% of the earth's surface is composed of water in the form of oceans, seas and lakes. Therefore determining the interactions of the atmosphere and the sea is imperative for global and long-term weather predictions. The tropics, which is considered to be a reservoir of moisture, is also the region where moisture convergence results in deep convection and associated mesoscale and regional scale disturbances that influence the global weather.

Air–sea interaction measurements are inherently more difficult than their overland counterparts because of the scarcity and the uneven geographical distribution of platforms from which measurements could be made. In the early years, an important step from marine meteorology towards air–sea interaction was based on observations of pilot balloon ascents made from ships of opportunity crossing the Atlantic Ocean. In the 1960s, the emphasis shifted from pilot balloon observations to larger scale field experiments (Hasse, 1990) heralding the beginning of an era of large international field experiments with an emphasis on studying the tropical oceans.

In the last two to three decades the structure of the Marine Atmospheric Boundary Layer (MABL) over the equatorial Pacific and Atlantic Ocean have been studied extensively during the field experiments that include the Atlantic Trade-wind Experiment (ATEX), Global Atmospheric Research Program Atlantic Tropical Experiment (GATE), tropical ocean global atmosphere (TOGA), TOGA and Coupled Ocean Atmosphere Response Experiment (TOGA–COARE) etc. (Hasse, 1990; Smith et al., 1996 and the references cited therein). However only a limited number of observational sets of data are available on the MABL over the Indian Ocean. Because of lack of coordinated field experiments, the structure and characteristics of MABL over the Indian Ocean are not fully understood. In this regard, the Indian Ocean Experiment (INDOEX) campaign has provided very valuable meteorological data. The experiment was carried out in four consecutive phases during 1996–1999. The main objective of the INDOEX

* Corresponding author. Tel.: + 91-471-562553; fax: +91-471-415335.

E-mail addresses: subbu_dbs@yahoo.com (D.B. Subrahamanyam), radhika@md3.vsnl.net.in (R. Ramachandran).

1364-6826/02/$ - see front matter
PII: S 1364-6826(01)00091-8

expedition was to study the radiative forcing by atmospheric aerosols and migration of anthropogenic and continental aerosols and pollutants over the Indian Ocean (Ramanathan et al., 1996). The preliminary results and detailed synthesis report on Indian component of INDOEX, IFP-99 campaign is already documented (Bahulayan et al., 2000; Mitra, 1999; Mitra et al., 2000). In the present study, the authors confine their research to the characteristics of the MABL.

The present study deals with the computation of air–sea fluxes over the Indian Ocean during INDOEX, IFP-99 campaign. Single level measurements of horizontal winds, air temperature and relative humidity in addition to Sea (skin) Surface Temperature (SST) are taken as the input data for the determination of drag coefficient (C_D), and sensible heat (C_H) and water vapor (C_E) exchange coefficients through an iterative scheme. The estimated values of these coefficients are used in the bulk aerodynamic method for computation of surface layer fluxes of momentum, heat and moisture.

2. Cruise details and data base

The INDOEX, which is a major international field experiment and research programme, involves concerted efforts of many scientists from various organizations. To address the multifaceted objectives of INDOEX, observations over a fairly large domain became necessary. After meeting the scientific requirements of the various participating groups, the cruise track of INDOEX, IFP-99 (SK-141 cruise) campaign was finalized. Fig. 1 shows the cruise track of INDOEX, IFP-99 campaign conducted onboard Oceanic Research Vessel (ORV) Sagar Kanya during January 20–March 12, 1999. From the figure, one can see that the INDOEX, IFP-99 campaign covered a broad oceanic region of the Indian Ocean and Central Arabian Sea over a latitude range 15°N–20°S and a longitude range 63°E–77°E. The track covered between Goa (India) to Port Louis (Mauritius) during January 20–February 11, 1999 (indicated by arrows in Fig. 1) is referred to as the forward track, whereas the track between Port Louis (Mauritius) to Goa (India) during February 17–March 12, 1999 is referred to as the return track of the cruise in this paper.

In Fig. 1, two meridional and two zonal tracks can be seen. The first meridional track along 77°E longitude (hereafter, referred to as track-I) was traversed between January 20 and February 04, 1999 during the forward track, whereas the second meridional track along 63°E longitude (hereafter, referred to as track-III) took place between February 18 and March 01, 1999 during the return track of the cruise. Similarly, there are two zonal tracks, one during the forward track and the other during the return track of the cruise. The first zonal track along 20°S latitude (hereafter, referred to as track-II) was conducted during February 04–11, 1999 during the forward track, whereas the second zonal track along 15°N latitude (hereafter, referred to as track-IV) was

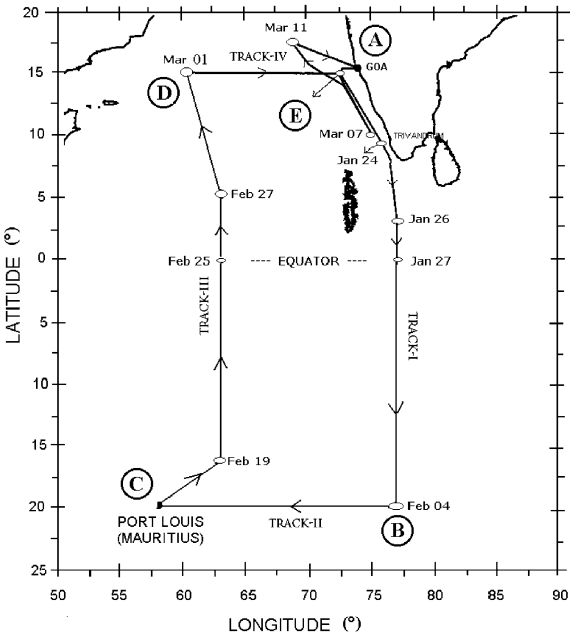

Fig. 1. Cruise track of INDOEX, IFP-99 (SK-141) cruise.

covered between March 01 and 06, 1999 during the return track of the cruise. We will be discussing the spatial variation of air–sea fluxes for all the four tracks separately.

3. Experimental set-up

Meteorological sensors were mounted onboard ORV Sagar Kanya on a 7-m long retractable boom close to the ship bow at two levels, 10 and 11-m above the sea surface. Three axis Gill propeller anemometers, sonic anemometer and fast response air-temperature sensors were among the fast response sensors, whereas pyranometers (for short wave and long wave radiation studies) and humicap (for measuring relative humidity and air temperature) sensors were among the slow response sensors. Fig. 2 shows the different sensors mounted on the boom onboard ORV Sagar Kanya. The fast response sensors along with the humicap sensor were mounted at 10-m level, whereas the pyranometers were mounted at 11 m. Data were acquired at the rate of 0.1 Hz from slow response sensors, and at 10 Hz from fast response sensors. Beside these, dry and wet bulb temperature (DBT and WBT), surface pressure and SST were measured manually at every 2-h interval. Psychrometer was used for measuring the DBT and WBT. SST was measured using the InfraRed (IR) thermometer. The IR thermometer used in the campaign had a resolution of 0.1°C, and its operating environmental limits lie in the range −20°C – 50°C. It provides a two-digit thumbwheel switch for adjusting its emissivity from 0.1 to 0.99. For the measurement of SST

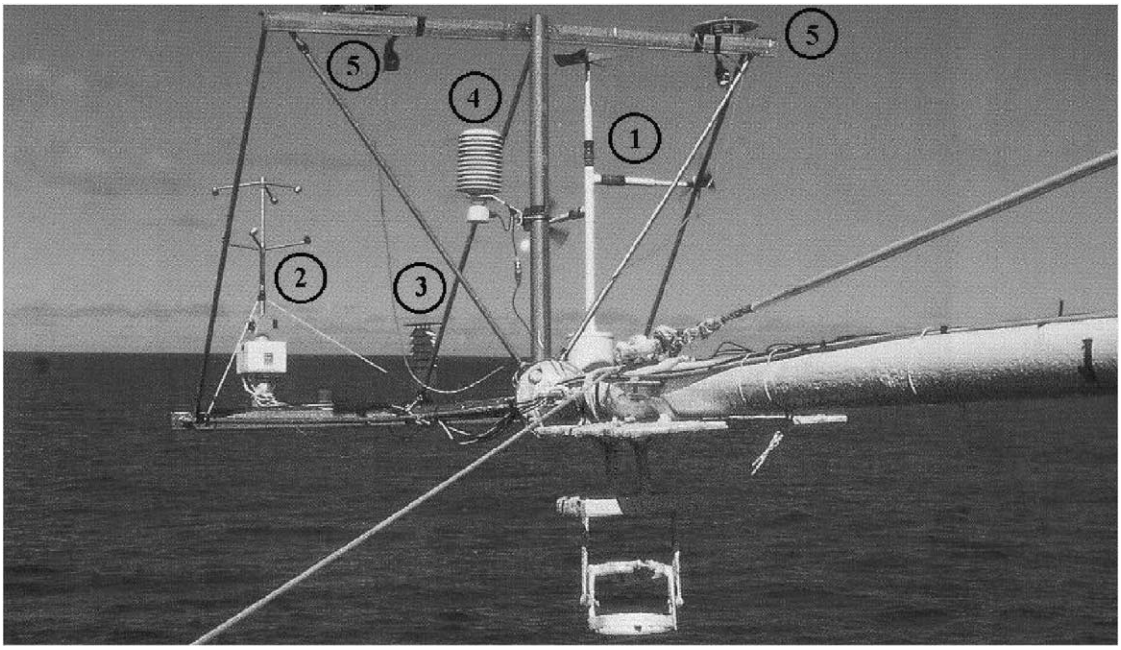

Fig. 2. Meteorological sensors mounted on retractable boom onboard ORV Sagar Kanya: (1) Gill propeller anemometer, (2) sonic anemometer, (3) fast response air temperature sensor, (4) humicap, (5) pyranometers.

Table 1
Accuracy of measurement of a few sensors

Serial no.	Sensor/instrument	Measured parameter	Manufacturer	Accuracy
1.	Gill propeller anemometer	U, V and W	RM Young, Michigan 49686, USA	0.1 m s^{-1}
2.	Humicap	Air temperature relative humidity	RM Young, Michigan 49686, USA	0.3°C for air temperature and 3% for relative humidity
3.	IR thermometer	Sea (skin) surface temperature	Telatemp Fullerton CA 92635, USA	0.5°C

during the campaign, the emissivity was set as 0.95. For the present study, hourly average values of air temperature and relative humidity measured from humicap sensor and horizontal winds measured from Gill propeller anemometers are used. The operating environmental limits for the humicap sensor lie in the range $-10°C-60°C$ for air temperature and $0-100\%$ for relative humidity. The details of a few sensors used in the present study are briefly tabulated in Table 1. Details on the accuracies of the measurements made by the sensors and the data acquisition system are reported elsewhere (Subrahamanyam et al., 2001a,b).

4. Method of analysis

There are four basic types of platforms for conducting flux measurements over the sea surface: aircrafts, buoys, towers, and ships. Each imposes its own set of limitation on the type and quality of the measurements. The present analysis is based on the computation of air–sea fluxes from a shipboard platform. A shipboard platform produces two main sources of error in flux measurement, which are not normally encountered over land, viz: local flow distortion over the bulk of the ship, and contamination of the wind sensors by heat and moisture. Apart from the gross contamination of wind components by the ship motion, the angular rotation of the instrument axes by pitch and roll cause cross-contamination of horizontal and vertical flux components (Bradley et al., 1991). As discussed in the previous section, the sensors were mounted on a retractable boom, extended forward from the bow of the ship (Subrahamanyam et al., 2001a,b); and can therefore produce errors in the measurements. The experimental setup used in the present campaign provided relatively good sampling for periods when winds were blowing

directly toward the bow of the ship; but when the winds are blowing from the stern, the data itself may be contaminated by heat and moisture originating from the ship. For correcting the wind speeds for flow distortion, we have identified three basic cases: the first, when the winds are blowing towards the bow of the ship, the second the winds are blowing along the stern, and the third case is when winds appear from either sides of the ship, and the respective corrections were made. However, it is to be noted that throughout the campaign, the average speed of ship itself was only about 3.75 Knots ($=1.93\ \mathrm{m\ s^{-1}}$); not very significant enough to contaminate the wind measurements. We could not, however, ascertain the effects on the measurements due to contamination by heat and moisture originating from the ship.

For the determination of the surface layer fluxes in Atmospheric Boundary Layer (ABL), four principal measurement techniques, viz: eddy correlation, profile, dissipation and bulk aerodynamic method are employed. The eddy correlation technique provides direct measurement of the fluxes and is considered as the most accurate method for computation of surface layer fluxes (Blanc, 1987; Stull, 1988). The other three techniques are semi-empirical, or indirect estimates. Computation of surface layer fluxes using eddy correlation method requires accurate measurement of vertical winds, air temperature and relative humidity at the same measurement height using fast response sensors (Kaimal and Finnigan, 1994; Kunhikrishnan et al., 1993; Radhika et al., 1994; Subrahamanyam et al., 2001b). However adoption of the eddy correlation method for computation of air–sea fluxes over ocean is quite difficult because of the constraints described earlier for ship borne platforms viz. non-availability of a stable platform over the sea surface. We have estimated the air–sea fluxes over Indian Ocean by adopting the bulk aerodynamic method. With a few notable exceptions, most of the experiments conducted to develop the bulk method use profile-derived flux determinations as the measurement standard (Blanc, 1987). However, Akkarappuram and Raman (1988) compared the estimated values of friction velocities over Atlantic Ocean by the bulk aerodynamic method with those estimated through dissipation and eddy correlation method, and they found a fairly good agreement between the two.

The bulk aerodynamic method estimates the turbulent exchanges of downward momentum flux or stress (τ) in $\mathrm{N\ m^{-2}}$, and sensible heat flux (H_S) and latent heat flux (H_L) in $\mathrm{W\ m^{-2}}$. Blanc (1987) provided an exhaustive analysis on the accuracies and uncertainties of air–sea fluxes computed through the bulk aerodynamic method over different oceanic regions, and also the different sources of errors while adopting the same. This method has been widely used throughout the marine and air–sea interaction studies for more than three decades now. Computation of surface layer fluxes using the bulk aerodynamic method requires determination of the exchange coefficients (C_D, C_H and C_E). Considerable effort has gone into the empirical determination of these exchange coefficients; Blanc (1985) compared several different schemes, and Smith (1989) provided a careful up-to-date review of the situation regarding measurement of evaporation. Said and Druilhet (1991) gave an exhaustive survey on the aerodynamic coefficients estimated through different methods over different oceanic regions during various field experiments. In the present analysis, we have estimated the values of exchange coefficients C_D, C_H and C_E through an iterative scheme based on the method suggested by Smith (1988). The detailed methodology and equations involved in the estimation of surface layer fluxes using this method are described below.

4.1. Estimation of friction velocity (u_*) and scaling temperature (θ_*)

In the atmospheric surface layer, fluxes of momentum, heat and moisture are assumed to be approximately constant, and the mean values of horizontal wind speed, potential temperature, and water vapor density are expected to vary logarithmically with height above the surface for near neutral density stratification. Empirical formulas were derived to account for deviations in the profiles from purely logarithmic in the diabatic case where the density stratification of the layer is different from that for the neutral case (Businger et al., 1971). The integrated forms of these profile relations are given as

$$U_{10} - U_S = (u_*/k)[\ln(z/z_0) - \psi_m], \tag{1}$$

$$\theta_{10} - T_S = (\theta_*/k)[\ln(z/z_{0t}) - \psi_t], \tag{2}$$

$$q_{10} - q_S = (q_*/k)[\ln(z/z_{0q}) - \psi_q], \tag{3}$$

where U, θ and q represents the mean wind speed ($\mathrm{m\ s^{-1}}$), potential temperature (K) and specific humidity ($\mathrm{kg\ kg^{-1}}$) respectively. The subscripts '$_S$' and '$_{10}$' represents the measurements of the concerned parameter at the sea surface and measurement height, z ($=10$ m) respectively, T_S is the sea surface temperature (K), k ($=0.4$) is von Karman constant, u_* is the friction velocity, θ_* and q_* are the scaling parameters for temperature and humidity, respectively. In Eqs. (1)–(3) the terms 'ψ'_m, 'ψ_t' and 'ψ_q' are the stability functions, whereas z_0, z_{0t} and z_{0q} are the roughness length for winds, temperature and humidity, respectively. To initialize the calculations, an estimated value of roughness length, $z_0 \approx 10^{-4}$ m is assumed applicable for the sea surface under moderate wind conditions (Lo, 1993). The values of roughness length for temperature and humidity (z_{0t} and z_{0q}) are determined as described below.

As per the definition of the neutral stability transfer coefficients for heat and moisture (C_{HN} and C_{EN}), Smith (1988) shows that these coefficients are approximately independent of wind speed with values of 1.15×10^{-3} at a reference height of 10 m. These transfer coefficients are given as

$$C_{HN} = k^2/[\ln(z/z_0)\ln(z/z_{0t})], \tag{4}$$

and

$$C_{EN} = k^2/[\ln(z/z_0)\ln(z/z_{0q})]. \quad (5)$$

Solving the above two equations with the prescribed value of C_{HN} and C_{EN} ($=1.15 \times 10^{-3}$) for z_{0t} and z_{0q}, we obtain

$$z_{0t} = z_{0q} = z/\exp[k^2/(1.15 \times 10^{-3})\ln(z/z_0)]. \quad (6)$$

Thus, with the initial values of z_0 ($\approx 10^{-4}$ m), and z_{0t} and z_{0q} estimated from Eq. (6), we estimate the values of friction velocity (u_*) and scaling parameters for temperature (θ_*) and humidity (q_*) with the help of the following equations:

$$u_* = [k(U_{10} - U_S)]/[\ln(z/z_0) - \psi_m], \quad (7)$$

$$\theta_* = [k(\theta_{10} - T_S)]/[\ln(z/z_{0t}) - \psi_t], \quad (8)$$

$$q_* = [k(q_{10} - q_S)]/[\ln(z/z_{0q}) - \psi_q]. \quad (9)$$

For the first iteration, the stability functions 'ψ_m', 'ψ_t' and 'ψ_q' are assumed to be zero and the wind speed at the sea surface (U_S) is taken as zero (Lo, 1993). The relative humidity at the sea surface is assumed to be 98% (Kraus and Businger, 1994) for the computation of specific humidity (q_S) at the sea surface.

4.2. Estimation of integrated stability functions (ψ_m and ψ_h)

As already defined in the above section, ψ_m, ψ_t and ψ_q are the integrated forms of the functions of the lower level stability (z/L), for wind speed, temperature and humidity, respectively. The integrated stability functions ψ_m, ψ_t and ψ_q for stable and unstable stratification are defined as (DeCosmo et al., 1996; Dyer, 1974; Smith, 1988)

$$\psi_m = \psi_t = \psi_q = -5(z/L) \quad (10a)$$

for stable stratification.

For unstable stratification, the integrated stability functions are defined as (DeCosmo et al., 1996; Paulson, 1970; Smith, 1988)

$$\psi_m = 2\ln[(1+x)/2] + \ln[(1+x^2)/2] - 2\tan^{-1}(x) + (\pi/2), \quad (10b)$$

$$\psi_t = \psi_q = 2\ln[(1+x^2)/2], \quad (10c)$$

where 'x' is given by

$$x = [1 - 16(z/L)]^{1/4}.$$

In the above equations, 'L' is the Monin–Obukhov stability length, and it has been derived using (Lo, 1993)

$$L = (T_V u_*^2)/(kg\theta_{V^*}), \quad (11)$$

where 'g' ($=9.8$ m s^{-2}) is the acceleration due to gravity. T_V (virtual temperature at the measurement height, in Kelvin) is used in order to include the effects of water vapor content on the density stratification, and θ_{V^*} is the scaling parameter for virtual temperature. It can be expressed in a manner similar to Eq. (8). In the above equations, the ratio (z/L) is called the stability parameter, and its value is positive in stable stratification and negative in unstable stratification. In near-neutral stability conditions, the stability functions vanish.

4.3. Estimation of roughness length (z_0)

With the estimates of friction velocity obtained from Eq. (7), we follow the empirical relation for roughness length suggested by Charnock (1955). For the open ocean, the roughness length, due mainly to the shorter surface waves, was postulated to depend on the surface stress based on dimensional considerations by Charnock (1955).

$$z_c = \alpha u_*^2/g, \quad (12a)$$

where α is an empirically determined constant. Results of numerous field experiments have verified this relationship, with slightly different values of the proportionality constant for open ocean measurements with a fully developed sea state (Wu, 1988). In the present analysis the value of α ($=0.011$) is assumed after Smith (1988), though Charnock (1958) suggested a value of $\alpha = 0.012$.

The roughness length for a smooth surface (e.g., Businger, 1973) depends on the viscosity and the friction velocity (Smith, 1988)

$$z_s = 0.11\nu/u_*, \quad (12b)$$

where the dynamic viscosity of air is $\nu = 14 \times 10^{-6}$ m^2 s^{-1}. The roughness length z_0, or in the other words, the virtual origin of the wind profiles, is obtained by adding z_c and z_s

$$z_0 = z_c + z_s. \quad (13)$$

The roughness length (z_0) estimate is then substituted into Eq. (6) to obtain the new estimates of roughness length for heat and moisture (z_{0t} and z_{0q}).

The wind speed at sea surface (U_S), commonly known as drift velocity, is generally believed to be zero. However, it has been verified both experimentally and theoretically that the surface drift velocity is approximately equal to u_* (e.g., Hicks, 1972; Lo, 1993; Roll, 1965). Therefore, for the ensuing iterations the estimated value of u_* is substituted in place of drift velocity (U_S) in all the calculations. Now, the estimated values of roughness length (z_0, z_{0t} and z_{0q}) and stability functions (ψ_m, ψ_t and ψ_q) are substituted into Eqs. (7)–(9) to determine the new estimates of u_*, θ_* and q_*.

With the new estimates of u_*, θ_* and q_*, stability functions (ψ_m, ψ_t and ψ_q) and roughness length (z_0, z_{0t} and z_{0q}) are determined again and the iteration is repeated between Eq. (6) and (13) until the u_*, θ_*, q_* and z_0 calculated from two consecutive iterations converge.

4.4. Determination of exchange coefficients (C_D, C_H and C_E) and the surface fluxes

The estimated values of u_*, θ_* and z_0 are then used for the computation of drag coefficient (C_D), and sensible heat (C_H) and water vapor (C_E) exchange coefficients (Byun, 1990; DeCosmo et al., 1996) using:

$$C_D = u_*^2/(U_{10} - U_S)^2, \tag{14}$$

$$C_H = u_*\theta_*/(U_{10} - U_S)(\theta_{10} - T_S), \tag{15}$$

$$C_E = u_* q_*/(U_{10} - U_S)(q_{10} - q_S). \tag{16}$$

Surface fluxes of momentum (τ), heat (H_S) and moisture (H_L) (De Cosmo et al., 1996) are then obtained by substituting C_D, C_H and C_E into

$$\tau = \rho C_D (U_{10} - U_S)^2, \tag{17}$$

$$H_S = \rho C_p C_H (U_{10} - U_S)(T_S - \theta_{10}), \tag{18}$$

$$H_L = \rho L_V C_E (U_{10} - U_S)(q_S - q_{10}), \tag{19}$$

where 'ρ' is the density of moist air, 'C_p' is the specific heat of moist air at constant pressure and 'L_V' is the latent heat of vaporization.

5. Results and discussion

5.1. Ambient meteorological conditions prevailing during the INDOEX, IFP-99 cruise

The meteorological conditions during the entire cruise can be summarized as follows: During the forward track of the cruise, most of the days were cloudy. Along track-I, heavy rains were observed in the latitude range 2–4°S. For tracks III and IV, i.e., the return track of the cruise, barring a few days, most of the days were clear, bright and sunny. The spatio-temporal variation of SST, air temperature, relative humidity and wind speed are shown in Fig. 3. Spatial variation of the above parameters for tracks I–IV are represented in the figure. The smallest division on the X-axis shown in Fig. 3 represents the temporal variation of these parameters for a day. All the four plots shown in Fig. 3 shows the

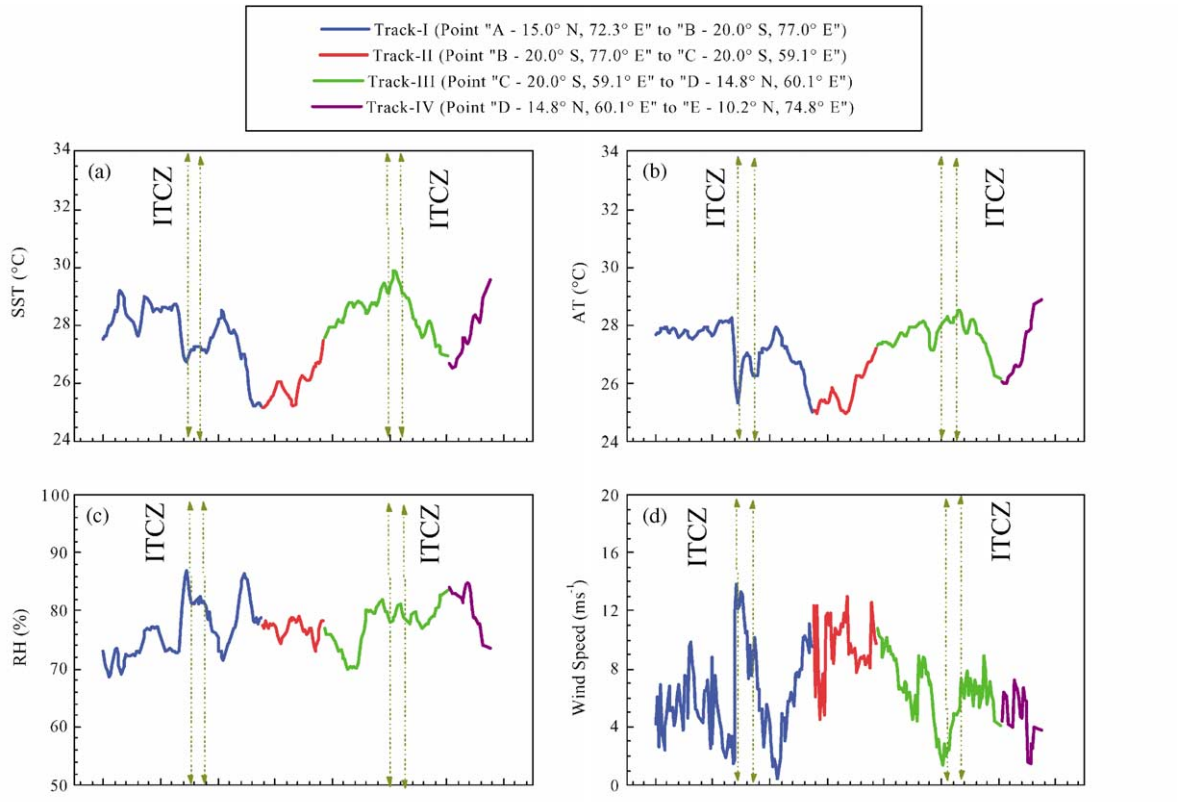

Fig. 3. Variation of the mean meteorological parameters during the cruise period of INDOEX, IFP-99 campaign.

temporal variation of these parameters during the entire cruise over a span of 52 days between January 21 and March 12, 1999. This excludes 7 days of stay in the Mauritius Island. The probable position of ITCZ for the forward track as well as return track is identified with the help of weekly averaged wind analysis provided by National Centre for Medium Range Weather Forecasting (NCMRWF, New Delhi, INDIA) plots (shown in Fig. 8), reported in INDOEX report (Madan et al., 1999). The position of ITCZ during the forward and return tracks is shown by a small belt in Fig. 3. It is to be noted that there was a change in the ambient meteorological conditions during the return track when compared to the forward track of the cruise. From Fig. 3a, we can see that the SST data collected during the entire cruise show variation in the range 25–32°C. The low values of SST (~27°C) observed over the ITCZ regions during the forward track of the cruise can be attributed to the cloudy and rainy weather prevailing in the region during that period, however during the bright sunny days of the return track, the ITCZ can be identified with the higher values of SST (in the range 29–30°C). The air temperature during the entire cruise varied within a range 24–33°C (Fig. 3(b)). The air temperature remained low (~26–27°C) over the ITCZ region during the forward track of cruise, and can be attributed to heavy rains observed over the region. However during the return track of cruise, the air temperature over the ITCZ region was relatively higher (~28°C) compared to the values observed for the forward track (Fig. 3b). The variation in relative humidity for the forward track was in the range 65–90%, whereas it varied between 70% and 90% for the return track of the cruise (Fig. 3c). High values of relative humidity (~90%) observed over the ITCZ regions during the forward track of the cruise can again be attributed to the precipitation observed over those regions (Fig. 3c). Fig. 3d shows the spatial and temporal variation of mean wind speed for the entire cruise. From Fig. 7d, it is obvious that during the entire forward track (tracks I and II) high values of wind speed were observed; whereas winds were relatively lower during the return track of cruise (tracks III and IV).

5.2. Calculated fluxes along the ship's tracks

The spatial variations of air–sea fluxes for the two meridional tracks, tracks I and III, are shown in Figs. 4 and 5, respectively. Similarly, the spatial variation of air–sea fluxes for the two zonal tracks, tracks II and IV, are shown in Figs. 6 and 7, respectively. Each of these figures are divided into four panels: the top three panels (a–c) represent the spatial variation of surface layer fluxes of heat (H_S), moisture (H_L) and momentum (τ) respectively, whereas the bottom panel (d) shows the corresponding variation of wind speed. We show the spatial variation of wind speed along with the surface layer fluxes, because of the possible wind speed dependence on the surface layer flux estimates, as given by Eqs. (17)–(19).

The latitudinal variation of air–sea fluxes and wind speed for meridional track-I is shown in Fig. 4. We can see from Fig. 4a that the sensible heat flux remains nearly constant with an average value of about 13 W m^{-2} throughout the track, except with a peak value of ~77 W m^{-2} at around 2–4°S (Fig. 4a). However, the latent heat flux shows large variations (Fig. 4b). The higher values of latent heat flux in the range 220–240 W m^{-2} observed around 2–4°S coincides with the peak observed for sensible heat flux. The momentum flux for track-I also shows a large peak at around 2–4°S (Fig. 4c). Further, the values of momentum flux and latent heat flux show an increasing trend in the Southern Hemisphere between 15 and 20°S (Figs. 4b and c) corresponding to increasing wind speeds. When these fluxes are compared with the variation of mean wind speed (Fig. 4d), we observe that the large peaks in the momentum flux and latent heat flux coincide with high values of wind speed observed over those latitudes. However, this is not the case for the sensible heat flux. Thus, we see that the latent heat flux and momentum flux show strong dependence on the wind speed, whereas such dependence is not prominent for the sensible heat flux estimates.

Fig. 5 shows the latitudinal variation of surface layer fluxes and wind speed for track-III covered during the return track. Just as for track-I, the sensible heat flux values are in the range 4–45 W m^{-2} for track-III (Fig. 5a). Low values of latent heat flux and momentum flux are seen around 1°N–3°S. It has to be noted that over the same latitude, low value of winds are also observed (Figs. 5b–d). On an average, the sensible heat flux was around ~18 W m^{-2}, whereas latent heat flux show variation within a range 35–260 W m^{-2}, with an average value of about 140 W m^{-2} for meridional track-III.

Fig. 6 shows the longitudinal variation of surface layer fluxes and wind speed for zonal track-II, during February 04–11, 1999. The sensible heat flux for track-II shows values in the range −2 to 57 W m^{-2}, with an average value of about 27 W m^{-2} (Fig. 6a). The estimated values of latent heat flux for track-II are in the range 70–215 W m^{-2}, with an average value of about 160 W m^{-2} (Fig. 6b), whereas the momentum flux values are in the range 0–0.3 N m^{-2}. Again we observe that the variation of latent heat flux and momentum flux for track-II are well in tune with the variation of wind speed. A sudden drop in the magnitude of wind speed (Fig. 6d) results in a considerable drop in the latent heat and momentum flux magnitudes for 74–75°E longitude (Figs. 6b and c). Such a significant effect is not seen however in the sensible heat flux estimates (Fig. 6a).

Fig. 7 shows the variation of the surface layer fluxes and wind speed for zonal track-IV, covered between March 01 and 06, 1999. We can see that almost all the estimated values of fluxes remained low without much variation (Figs. 7a–c). Winds also were low (~4.5 m s^{-1}) for track-IV (Fig. 7d).

Table 2 summarizes the spatial variation of the mean parameters (SST, air temperature, wind speed, relative humidity) and the surface layer fluxes of momentum, heat and

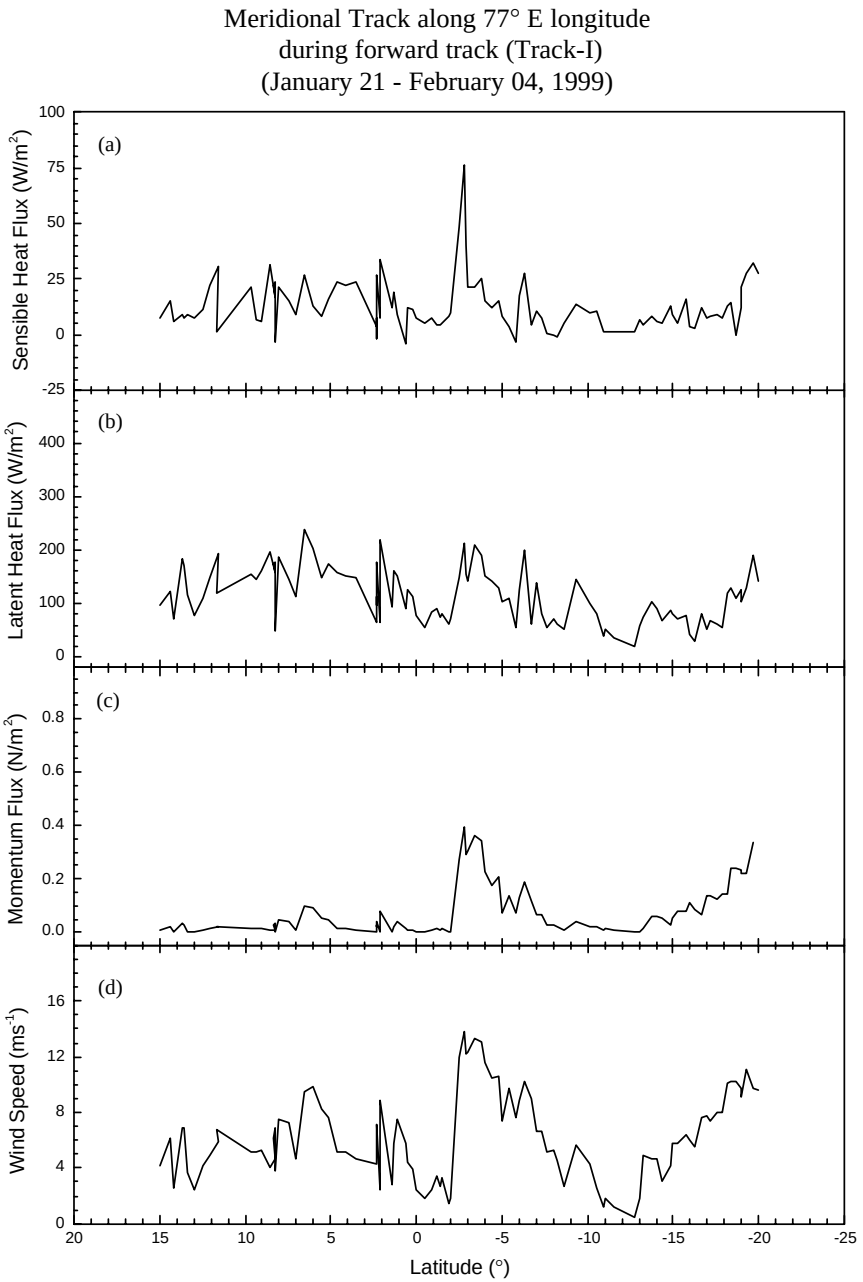

Fig. 4. Latitudinal variation of surface layer fluxes and wind speed for track-I: (a) sensible heat flux, (b) latent heat flux, (c) momentum flux and (d) wind speed.

moisture for tracks I–IV. The range of variation of these parameters for all the four tracks along with the average values for these tracks are shown in the table.

5.3. Fluxes in relation to NCMRWF wind analysis

The weekly averaged wind analysis provided by NCMRWF at 925 hPa over the Indian Ocean (Madan et al., 1999) roughly corresponding to the time periods of tracks I, II, III and IV, respectively are shown in Fig. 8a–d. The tracks are overlaid on the wind patterns for easy reference. Availability of two meridional tracks (tracks I and III) during the campaign provided an opportunity to study the MABL characteristics over the inter-tropical convergence zone (ITCZ). During the forward track, a strong convergence of winds is observed between 0 and 10°S along the track-I (77°E)

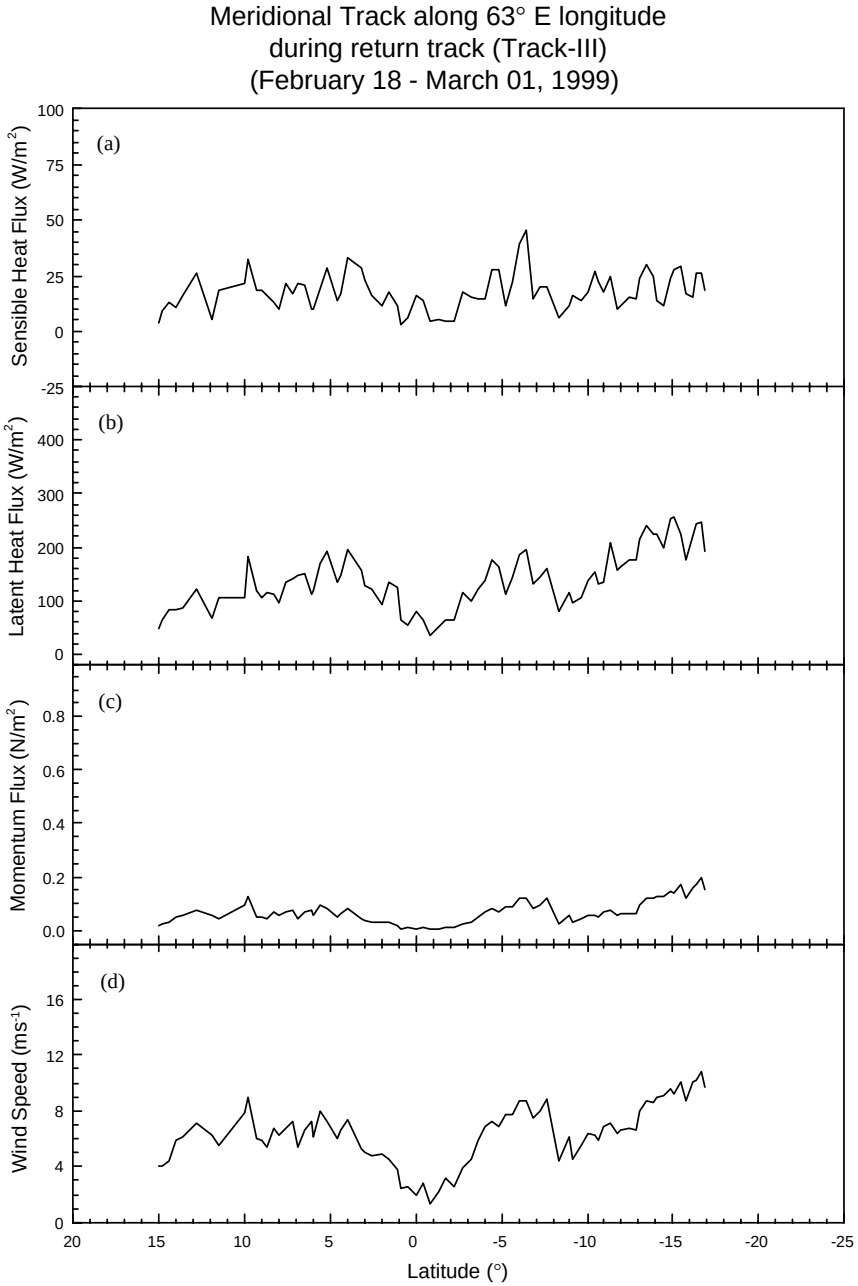

Fig. 5. Same as Fig. 4, but for track-III.

(Fig. 8a), whereas such convergence is not seen for track-III (63°E) (Fig. 8c). Similar observations are supported from the surface observations of winds shown in Fig. 3d. The magnitude of winds over the ITCZ region for track-I is high ($\sim$13 m s^{-1}), whereas it is quite low ($\sim$2–3 m s^{-1}) for track-III (Fig. 3d). It has to be noted that the observations shown in Fig. 3 are surface observations, whereas the wind field shown in Fig. 8 is for 925 hPa provided by NCMRWF. Strong convergence of trade winds between 0 and 10°S during track-I is due to existence of the ITCZ between those latitudes. However, convergence of trade winds along track-III is weak, indicating the weakening of ITCZ during the return track. The peak value of sensible heat flux ($\sim$77 W m^{-2}) observed along the track-I at 2–4°S can be a direct consequence of the strong convergence observed over those latitudes due to the presence of ITCZ, as seen

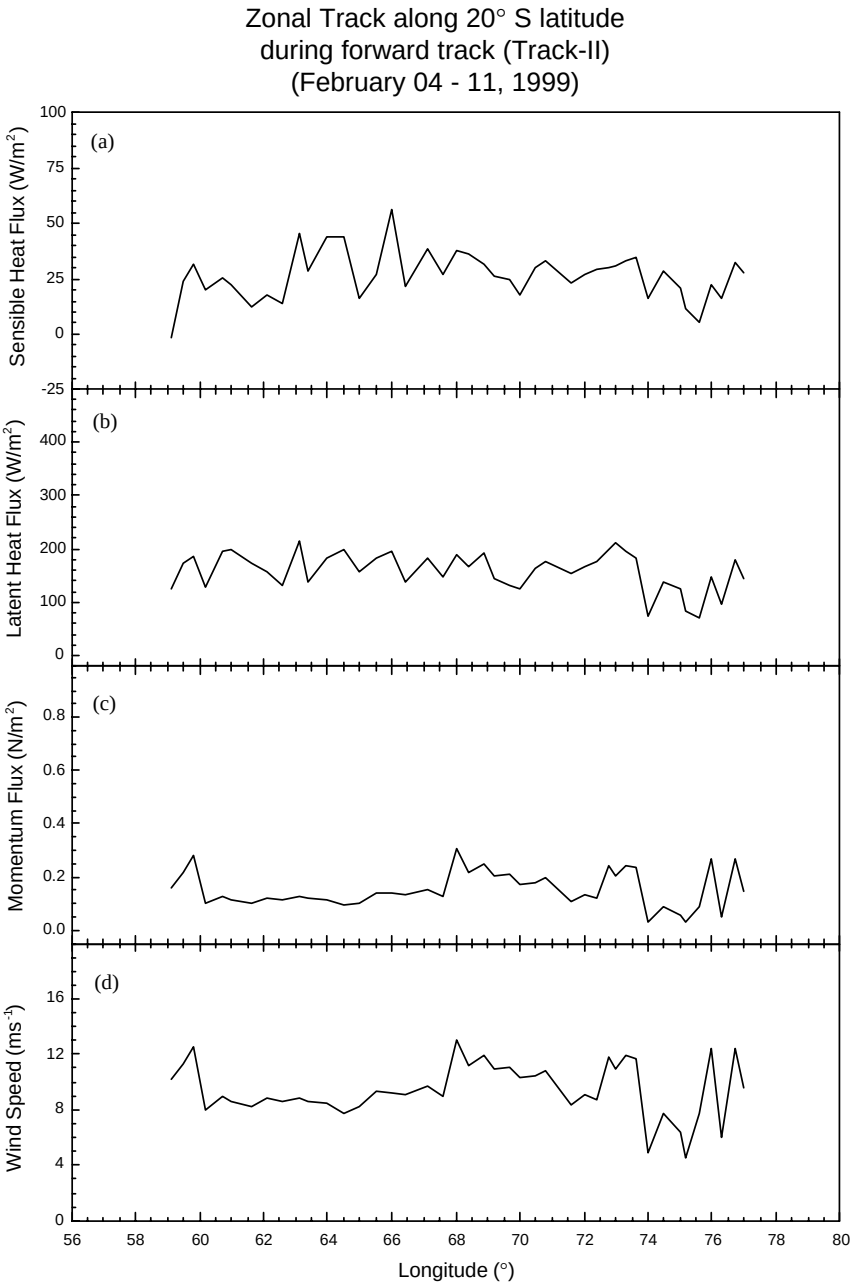

Fig. 6. Longitudinal variation of surface layer fluxes and wind speed for track-II: (a) sensible heat flux, (b) latent heat flux, (c) momentum flux and (d) wind speed.

in Fig. 8a. This perhaps explains the peak value of sensible heat flux ($\sim$77 W m^{-2}) observed in those latitude regions.

When we compare the variation of air–sea fluxes observed along track-IV with that observed along track-II, a considerable difference in the pattern of variation can be observed between the two. We find large variations in all the parameters for track-II, whereas a more or less constant behavior is observed in almost all the parameters for track-IV. It is to be noted that track-II (lying in the Southern Hemisphere) was traversed during the Southern Hemispheric summer when high convective activity prevailed in the region with wind speeds of about 9.5 m s^{-1} as compared to track-IV during March, when the wind speeds were only $\sim$4.5 m s^{-1} (Figs. 8b and d). From Table 2 also we can see that the estimates

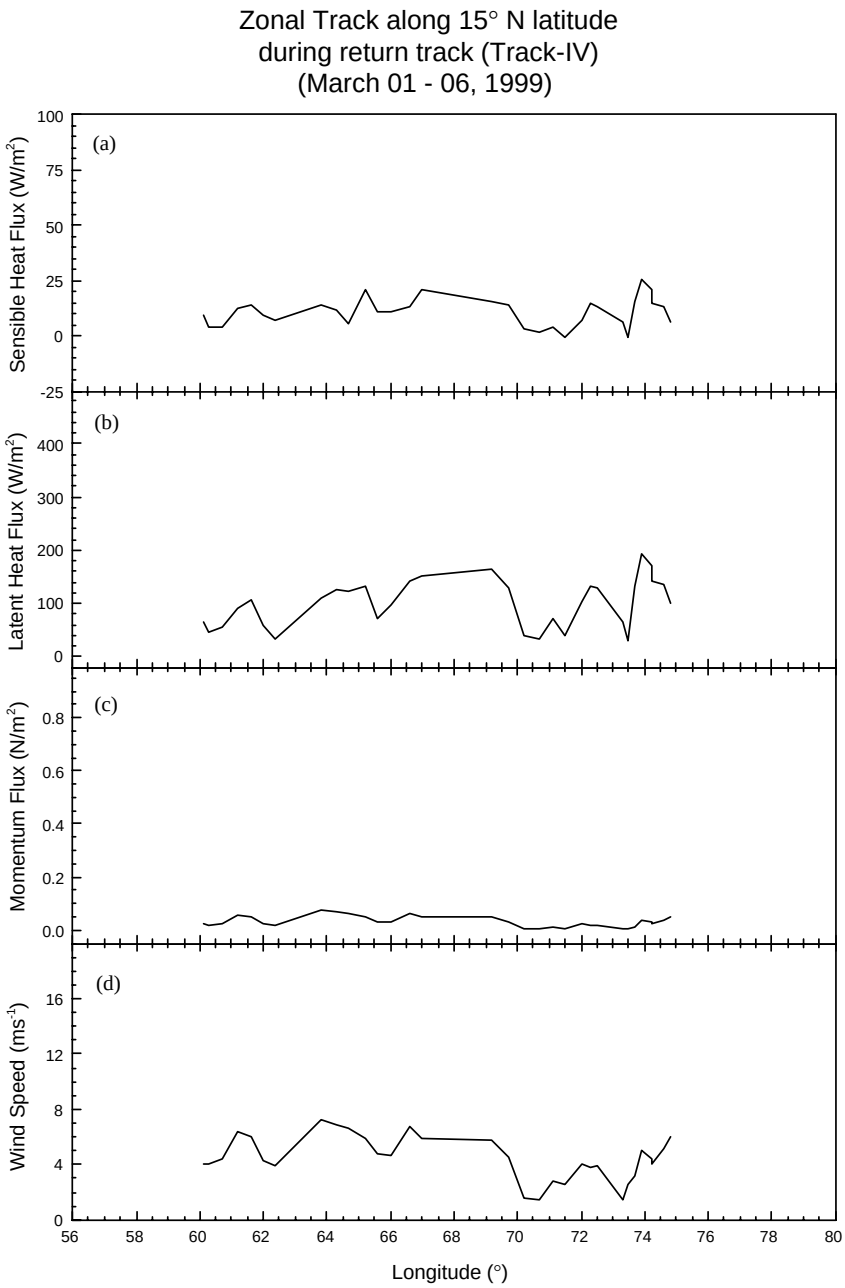

Fig. 7. Same as Fig. 6, but for track-IV.

of fluxes for track-II are comparatively higher to those for track-IV. The sensible heat flux was around 27 W m^{-2} for track-II, whereas it was low ($\sim$10 W m^{-2}) for track-II. Similar observations can be seen for latent heat flux estimates also and it can be attributed to the prevailing conditions in that location. Observational studies over the Arabian Sea coast (Prakash et al., 1992) suggest the month of March to be a transition period from winter monsoon to summer monsoon for the Indian sub-continent. We presume therefore that the changed ambient weather conditions in March could possibly affect the flux estimates too. The magnitudes of the wind speed observed for track-IV are considerably low, $\sim$4.5 m s^{-1}, typical of the season. Low values of winds observed for the track-IV is one of the reasons for the low

Table 2
Spatial variation of the mean parameters and fluxes for the four cruise tracks

Parameter		Track-I	Track-II	Track-III	Track-IV	Entire cruise
SST	Range	25.0–29.6	25.0–27.1	26.3–30.5	26.0–31.7	25.0–31.7
(°C)	Mean	27.7	25.9	28.4	28.5	27.9
Air temperature	Range	23.6–30.5	23.8–28.4	25.6–30.4	25.8–32.6	23.6–32.6
(°C)	Mean	27.3	25.5	27.6	27.9	27.3
Wind speed	Range	1.2–13.8	4.6–13.0	1.3–10.8	1.5–7.2	1.2–13.8
($m\ s^{-1}$)	Mean	6.3	9.5	6.4	4.5	6.8
Relative humidity	Range	65.5–91.9	70.8–83.0	68.7–86.5	69.5–89.4	65.5–91.9
(%)	Mean	76.7	77.0	78.0	77.4	77.0
Momentum flux	Range	0.002–0.360	0.029–0.304	0.003–0.196	0.003–0.077	0.002–0.360
($N\ m^{-2}$)	Mean	0.077	0.154	0.069	0.032	0.084
Sensible heat flux	Range	−3.9–76.2	−1.3–56.2	3.5–45.2	−0.8–25.2	−3.9–76.2
($W\ m^{-2}$)	Mean	12.9	26.5	17.8	10.7	17.0
Latent heat flux	Range	29.3–237.0	71.0–214.1	34.4–257.3	30.5–192.6	29.3–276.3
($W\ m^{-2}$)	Mean	116.7	159.3	139.8	100.4	136.8

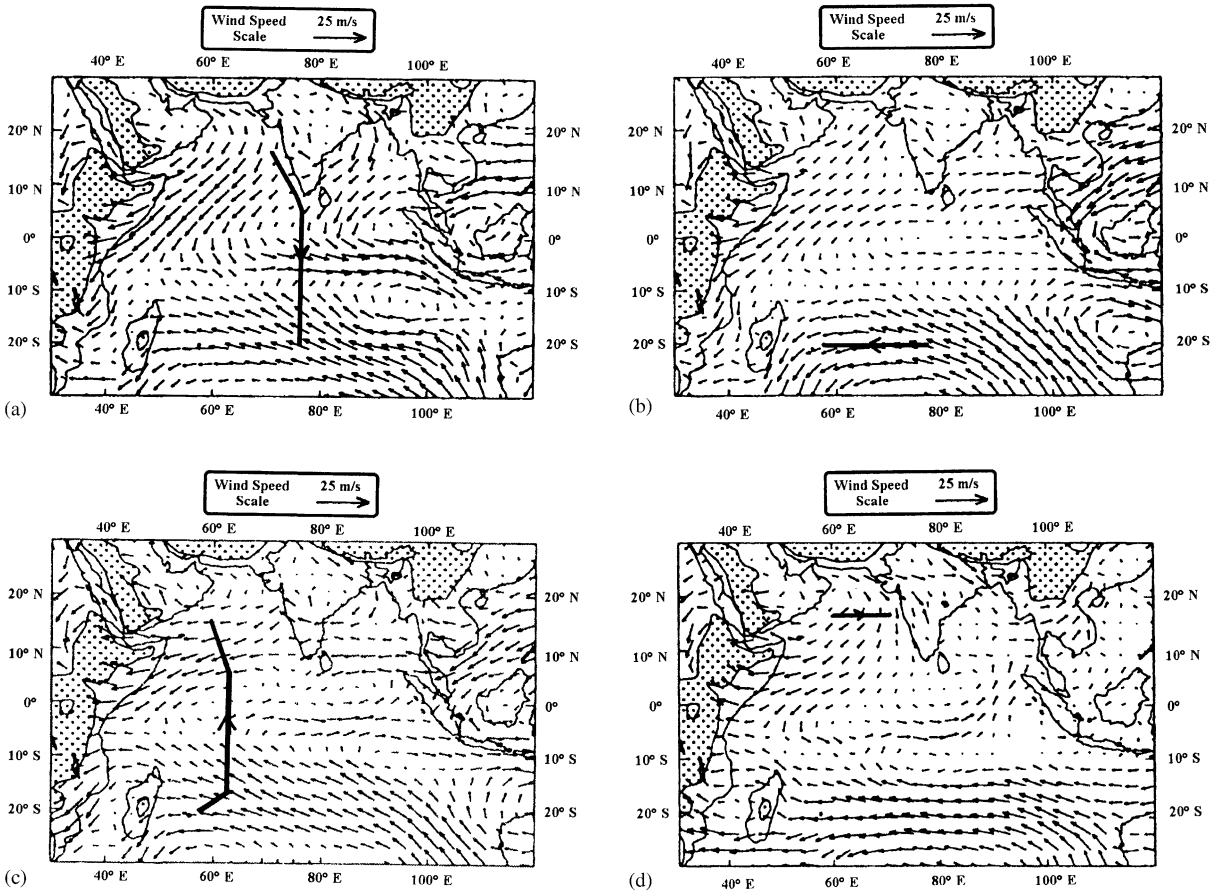

Fig. 8. (a)–(d) Weekly averaged winds at 925 hPa roughly corresponding to the tracks I, II, III and IV, respectively, obtained from National Centre for Medium Range Weather Forecasting (NCMRWF) wind analysis. The respective cruise tracks are superimposed with thick (continuous) lines over the wind patterns (courtesy: Madan et al., 1999).

values of momentum flux for that period. In addition to this, low values of sensible heat flux, as well as latent heat flux observed for track-IV can be attributed to weak convection prevailing in the region.

5.4. Comparison with TOGA–COARE surface fluxes

Estimates of air–sea fluxes were reported for the tropical western Pacific Ocean (Bradley et al., 1991; Godfrey et al., 1991). During the Tropical Ocean-Global Atmosphere Coupled Ocean-Atmosphere Response Experiment (TOGA-COARE) over tropical western Pacific Ocean, the estimates of surface layer fluxes were compared with the estimates made using satellite data (Clayson and Curry, 1996). Their estimates of momentum flux were in the range 0–0.25 N m^{-2}, the sensible heat flux was observed in the range -10 to 30 W m^{-2}, whereas the latent heat flux was observed in the range 25–250 W m^{-2} (Clayson and Curry, 1996). Our estimates of air–sea fluxes over Indian Ocean shows momentum flux in the range 0–0.4 N m^{-2}, sensible heat flux in the range -4 to 80 W m^{-2} and the latent heat flux in the range 30–280 W m^{-2} implying a wider range of values of the fluxes over the Indian Ocean.

The estimated values of momentum flux and latent heat flux over the Indian Ocean are considerably dependent on the magnitude of wind speed, whereas such dependence on wind speed is not significant for sensible heat flux. However, with increasing values of winds, the magnitude of sensible heat flux also increases. In general, high values of winds are observed over Southern Hemisphere whereas they were considerably low for Northern Hemisphere throughout the cruise. On an average, estimated values of fluxes for Southern Hemisphere are comparatively higher to those estimated for Northern Hemisphere. It can be attributed to the prevailing weather of the particular region since during the month of December–February, Northern Hemisphere experiences winter, with low convection whereas Southern Hemisphere experiences summer with relatively high convective activity.

5.5. Dependence of fluxes on wind speed

The dependence of the surface layer fluxes on wind speed could be better seen through the scatter plots (Figs. 9a–c). In general, all the fluxes (sensible heat flux, latent heat flux and momentum flux) show an increasing trend with increase in the magnitude of wind speed (Figs. 9a, b and c, respectively). However, such a trend is quite prominent for latent heat flux and momentum flux, but not for the sensible heat flux (Fig. 9a). For sensible heat flux and latent heat flux however, at higher wind speeds, there is more scatter. We notice a substantial increase in momentum flux values with wind speed with no scatter at high wind speeds, possibly because of the U^2 dependence of momentum flux, as given in Eq. (17).

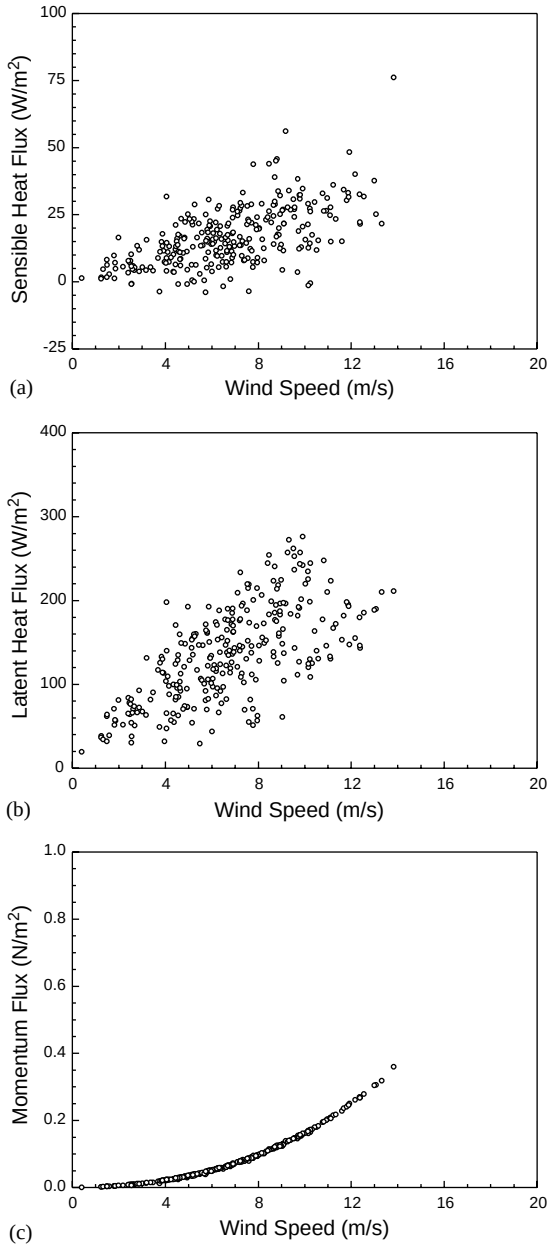

Fig. 9. Variation of surface layer fluxes with respect to wind speed: (a) sensible heat flux vs. wind speed, (b) latent heat flux vs. wind speed and (c) momentum flux vs. wind speed.

6. Concluding remarks

The INDOEX, IFP-99 campaign provided an opportunity to study the structure and characteristics of MABL over Indian Ocean. In this paper, we have addressed some of the features of air–sea interaction over the Indian Ocean by computing the surface layer fluxes of heat, moisture and

momentum. Air–sea exchange parameters of water vapor, heat and momentum are important inputs for mesoscale and GCM modelling. The latent heat flux is often the largest term in the heat balance of the upper ocean. However, sensible heat and water vapor fluxes have rarely been measured in moderate to high wind conditions over the ocean, and the underlying physics of these exchange processes over rough seas are still not very well understood.

Over the Indian Ocean region our study conducted during the INDOEX, IFP-99 campaign showed momentum flux in the range 0–0.4 N m^{-2}, sensible heat flux in the range -4 to 80 W m^{-2} and the latent heat flux in the range 30–280 W m^{-2}. The variations in the estimates are possibly related to the prevailing weather in the respective regions.

There are several studies that report MABL characteristics over oceans; such studies over the tropical Indian Ocean region, however, are few. The present study offers fairly reliable estimates of air–sea fluxes and air–sea exchange coefficients over the Indian Ocean. We believe that the results shown in this work are quite important for further studies on MABL over the Indian Ocean.

Acknowledgements

We acknowledge with thanks the help rendered by Dr. K. Sen Gupta, Former-Head, Boundary Layer Physics (BLP) Branch, Space Physics Laboratory (SPL), Vikram Sarabhai Space Centre (VSSC), Thiruvananthapuram for initiating the BLP component of the INDOEX programme. We would like to thank Dr. Stuart D. Smith and an anonymous reviewer, for their constructive comments that greatly improved the contents of this paper. Prof. R. Sridharan, Director, SPL, VSSC, Thiruvananthapuram and Dr. Prakash M. Dolas are also acknowledged for their critical appraisal of the manuscript. Sincere thanks are also due to Prof. G.S. Bhat and his colleagues, especially J.V.S Raju and C.P. Chandrashekhar, the cruise participants from Centre for Atmospheric and Oceanic Sciences (CAOS), Indian Institute of Science (IISc), Bangalore for their help at the time of installation of the sensors onboard ORV Sagar Kanya and also during the cruise. One of the authors, Subrahamanyam, who participated in the INDOEX, IFP-99 (SK-141) campaign is thankful to all the crewmembers of the ORV Sagar Kanya for their cooperation during the entire cruise.

References

Akkarappuram, A.F., Raman, S., 1988. A comparison of surface friction velocities estimated by Dissipation and Iterative Bulk Aerodynamic methods during GALE. Geophysical Research Letters 15, 401–404.

Bahulayan, N., Jayaraman, A., Rao, L.V.G., Viswanathan, G., Mitra, A.P., 2000. Report on INDOEX, IFP-99 Cruise of ORV SAGAR KANYA (SK-141), INDOEX-TR-01-2K. National Steering Committee, NPL, CSIR, Govt. of India, Dr K.S. Krishnan Marg, New Delhi, 52pp.

Blanc, T.V., 1985. Variation of bulk-derived surface flux, stability and roughness results due to the use of different transfer coefficient schemes. Journal of Physical Oceanography 15, 650–659.

Blanc, T.V., 1987. Accuracy of bulk-method-determined flux, stability, and sea surface roughness. Journal of Geophysical Research 92, 3867–3876.

Bradley, E.F., Coppin, P.A., Godfrey, J.S., 1991. Measurements of sensible and latent heat flux in the western equatorial Pacific Ocean. Journal of Geophysical Research 96, 3375–3389.

Businger, J.A., Wyngaard, J.C., Izumi, Y., Badgley, E.F., 1971. Flux profile relationships in the atmospheric surface layer. Journal of Atmospheric Sciences 28, 181–189.

Businger, J.A., 1973. Turbulent transfer in the atmospheric surface layer. In: Haugen, D.A (Ed.), Workshop on Micrometeorology. American Meteorological Society, Boston, MA, pp. 67–100.

Byun, D.W., 1990. On the analytical solutions of flux-profile relationships for the atmospheric surface layer. Journal of Applied Meteorology 29, 652–657.

Charnock, H., 1955. Wind stress on the water surface. Quarterly Journal of Royal Meteorological Society 81, 639–640.

Charnock, H., 1958. A note on empirical wind-wave formulae. Quarterly Journal of Royal Meteorological Society 84, 443–447.

Clayson, C.A., Curry, J.A., 1996. Determination of surface turbulent fluxes for the Tropical Ocean-Global Atmosphere Coupled Ocean-Atmosphere Response Experiment: comparison of satellite retrievals and in situ measurements. Journal of Geophysical Research 101, 28 515–28 528.

DeCosmo, J., Kastaros, K.V., Smith, S.D., Anderson, R.J., Oost, W.J., Bumke, K., Chadwick, H., 1996. Air–sea exchange of water vapor and sensible heat: the humidity exchange over the sea (HEXOS) results. Journal of Geophysical Research 101, 12 001–12 016.

Dyer, A.J., 1974. A review of flux-profile relationships. Boundary Layer Meteorology 7, 363–372.

Godfrey, J.S., Nunez, M., Bradley, E.F., Coppin, P.A., Lindstorm, E.J., 1991. On the net surface heat flux into the western equatorial Pacific. Journal of Geophysical Research 96, 3391–3400.

Hasse, L., 1990. Oceanic micrometeorological field experiments: an historical perspective. Boundary Layer Meteorology 50, 139–146.

Hicks, B.B., 1972. Some evaluations of drag and bulk transfer coefficients over water bodies of different size. Boundary Layer Meteorology 3, 201–213.

Kaimal, J.C., Finnigan, J.J., 1994. Atmospheric Boundary Layer Flows: Their Structure and Measurement, Oxford University Press, Inc., New York, 289pp.

Kraus, E.B., Businger, J.A., 1994. Atmosphere–Ocean Interactions, 2nd Edition. Oxford University Press, Oxford, 352pp.

Kunhikrishnan, P.K., Sen Gupta, K., Radhika, R., Prakash, J.W.J., Narayanan Nair, K., 1993. Study on thermal internal boundary layer structure over Thumba, India. Annales Geophysicae 11, 52–60.

Lo, A.K-F., 1993. The direct calculation of fluxes and profiles in the marine surface layer using measurements from a single atmospheric level. Journal of Applied Meteorology 32, 1893–1900.

Madan, O.P., et al., 1999. Meteorological Analysis during INDOEX, Intensive Field Phase—1999, Vol. II, Wind Analysis

and Trajectories. Centre for Atmospheric Sciences, IIT Delhi, Hauz Khas, New Delhi.

Mitra, A.P., 1999. INDOEX (India): introductory note. Current Science 76, 886–889.

Mitra, A.P., Jayaraman, A., Krishnamurthy, B.V., Mohanty, U.C., Viswanathan, G., 2000. INDOEX—India Program Synthesis Report, INDOEX-TR-02-2K. National Steering Committee, NPL, CSIR, Govt. of India, Dr K.S. Krishnan Marg, New Delhi, 52pp.

Paulson, C.A., 1970. The mathematical representation of wind speed and temperature profiles in the unstable atmospheric surface layer. Journal of Applied Meteorology 9, 857–861.

Prakash, J.W.J., Radhika, R., Narayanan Nair, K., Sen Gupta, K., Kunhikrishnan, P.K., 1992. On the structure of sea breeze fronts observed near the coast line of Thumba. Boundary Layer Meteorology 59, 111–124.

Radhika, R., Prakash, J.W.J., Sen Gupta, K., Narayanan Nair, K., Kunhikrishnan, P.K., 1994. Variability of surface roughness and turbulence intensities at a costal terrain in India. Boundary Layer Meteorology 70, 385–400.

Ramanathan, V., et al., 1996. Indian Ocean Experiment (INDOEX); A multi-agency proposal for Field Experiment in the Indian Ocean. C^4 Publication No. 162, Scripps Institution of Oceanography, La Jolla, CA, 1996; also at (http://www.indoex.ucsd.edu).

Roll, H.U., 1965. Physics of the Marine Atmosphere, Academic Press, New York, 426pp.

Said, F., Druilhet, A., 1991. Experimental study of the atmospheric marine boundary layer from in-situ aircraft measurements (TOSCANE-T CAMPAIGN): variability of boundary conditions and Eddy flux parameterization. Boundary Layer Meteorology 47, 277–293.

Smith, S.D., 1988. Coefficients for sea surface wind stress, heat flux, and wind profiles as a function of wind speed and temperature. Journal of Geophysical Research 93, 15 467–15 472.

Smith, S.D., 1989. Water vapor flux at the sea surface. Boundary Layer Meteorology 47, 277–293.

Smith, S.D., Fairall, C.W., Geernaert, G.L., Hasse, L., 1996. Air–sea fluxes: 25 years of progress. Boundary Layer Meteorology 78, 247–290.

Stull, R.B., 1988. An Introduction to Boundary Layer Meteorology. Kluwer Academic Publishers, AA Dordrecht, The Netherlands, 666pp.

Subrahamanyam, D.B., Sen Gupta, K., Ravindran, S., Kunhikrishnan, P.K., Ramachandran, R., Ramana, M.V., Krishnan, P., 2001a. Variation of marine atmospheric boundary layer parameters in the latitude range 15°N to 20°S and longitude range 63°E to 77°E during INDOEX, IFP-99. Proceedings of the Symposium TROPMET 2000 on Ocean Atmosphere held at Kochi, IMS, CUSAT, Cochin, Kerala, India, 1–4 February, pp. 410–414 (Cochin Chapter).

Subrahamanyam, D.B., Sen Gupta, K., Ravindran, S., Krishnan, P., 2001b. Study of sea breeze and land breeze along the west coast of Indian sub-continent over the latitude range 15°N to 8°N during INDOEX IFP-99 (SK-141) cruise, Current Science (Supplement), 80 (Suppl.), 85–88.

Wu, J., 1988. On nondimentional correlation between roughness length and wind-friction velocity. Journal of Oceanographical Society of Japan 44, 254–260.